Nanoscale

Accepted Manuscript

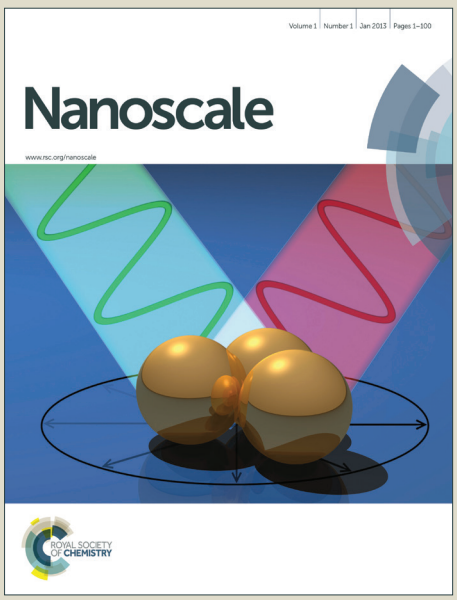

ROYAL SOCIETY OF CHEMISTRY

www.rsc.org/nanoscale

Measuring binding kinetics of aromatic thiolated molecules with nanoparticles *via* surface-enhanced Raman spectroscopy

Brent M. DeVetter,[a,b] Prabuddha Mukherjee,[b] Catherine J. Murphy[c] and Rohit Bhargava[a,b,c,d,e]

[a]Department of Electrical and Computer Engineering, [b]Beckman Institute for Advanced Science and Technology, [c]Department of Chemistry, [d]Department of Bioengineering, [e]Department of Mechanical Science and Engineering, University of Illinois at Urbana-Champaign, Urbana, IL, 61801.

Corresponding author: rxb@illinois.edu

Abstract

Colloidal plasmonic nanomaterials, consisting of metals such as gold and silver, are excellent candidates for advanced optical probes and devices, but precise control over surface chemistry is essential for realizing their full potential. Coupling thiolated (R-SH) molecules to nanoprobe surfaces is a convenient and established route to tailor surface properties. The ability to dynamically probe and monitor the surface chemistry of nanoparticles in solution is essential for rapidly manufacturing spectroscopically tunable nanoparticles. In this study, we report the development of surface-enhanced Raman spectroscopy (SERS) as a method to monitor the kinetics of gold-thiolate bond formation on colloidal gold nanoparticles. A theoretical model combining SERS enhancement with the Beer-Lambert law is proposed to explain ensemble scattering and absorption effects in colloids during chemisorption. In order to maximize biological relevance and signal reproducibility, experiments used to validate the model focused on maintaining nanoparticle stability after the addition of water-soluble aromatic thiolated molecules. Our results indicate that ligand exchange on gold nanoparticles follow a first-order Langmuir adsorption model with rate constants on the order of 0.01 min^{-1}. This study demonstrates an experimental spectroscopic method and theoretical model for monitoring binding kinetics that may prove useful for designing novel probes.

KEYWORDS: surface-enhanced Raman spectroscopy, plasmonics, ligand exchange, gold-thiol binding kinetics

Introduction

Precise control over nanoscale features has produced many exciting advances in electronic, photonic, and biomedical devices over the last two decades.[1–3] Integral to these advances has been the realization that control over the surface chemistries of both macroscopic substrates and nanoscopic probes is crucial for the development of new and existing nanotechnologies. Molecules containing thiol (R-SH) moieties are particularly well-suited for engineering surface chemistries due to the covalent nature of metal-sulfur bonds (~130 kJ/mol for Au-S).[4] Researchers have demonstrated thiol's ubiquitous nature through applications such as the preparation and functionalization of plasmonic nanocrystals,[5] semiconductor quantum dots,[6] and self-assembled monolayers.[7] Rigorous investigation of the metal-thiolate bond is essential for the development of nanotechnologies with unprecedented surface control.

For biological sensing applications, gold nanoparticles are commonly synthesized in aqueous wet chemistry with stabilizing ligands including polyvinylpyrrolidone (PVP), citrate, cetyltrimethylammonium bromide (CTAB), and cetyltrimethylammonium chloride (CTAC). Most notably, the surfactant CTAB can have growth directing properties leading to the formation of anisotropic nanostructures such as gold nanorods and gold nanoplates.[8] The relative strength of the bond between the stabilizing ligands and the gold surface affects our ability to functionalize nanoparticles for biological sensing applications. In highly ionic tissue microenvironments consisting of proteins and varying degrees of pH, it is especially important to have complete control over the probe's surface chemistry. For example, nanoprobes are often coated in thiolated polyethylene glycol in order to increase circulation time and biocompatibility by partially masking probes from proteins found in biological tissues and serum.[5] Bifunctionalized polyethylene glycol molecules with reactive functional groups, such as

carboxylic acid, are frequently coupled to proteins, aptamers, or other biomolecules for targeting applications.[9,10] Unlike electrostatically bound reporter molecules, covalently bound reporter molecules are not susceptible to diffusion and are significantly more reliable for long-term biological studies. In a similar vein, the efficiency of ligand exchange of thiolated polyethylene glycol is heavily dependent on the original stabilizing ligand,[11] with CTAB being recognized as the most difficult ligand to replace. Therefore, consideration of the as-synthesized stabilizing ligand for successful ligand exchange is essential.

Self-assembled monolayers (SAMs) were one of the earliest and most common techniques for controlling surface chemistry and fabricating nanopatterned substrates. SAMs form when free gas or liquid phase molecules spontaneously arrange as they adsorb to a surface. A popular choice for SAMs is alkanethiols; alkanethiols contain a thiol head group, which readily chemisorbs to gold, and an alkyl chain. The strength of the metal-thiolate bond makes thiol bearing molecules invaluable for applications involving metallic substrates. The structure and kinetics of alkanethiol SAM formation have been heavily characterized using diverse surface analysis techniques such as scanning tunneling microscopy, x-ray diffraction, atomic force microscopy, vibrational spectroscopy, and theoretically *via* density functional theory.[7,12] It is well established that alkanethiol SAM formation essentially follows the Langmuir isotherm.[13–15] The Langmuir isotherm assumes monolayer coverage, noninteracting adsorbed molecular species, uniform binding sites, and may be described by:

$$\theta = \frac{KC}{1 + KC} \quad [1]$$

where K is a constant, C is the concentration of the adsorbed species, and θ is fractional surface coverage. Understanding the kinetics of metal-thiolate bond formation is essential for rapidly manufacturing SAMs. To date, the majority of studies investigating thiol kinetics have focused on flat macroscopic substrate SAM formation.[12–14] Advances in the control over surface morphology of colloidal nanoparticles, however, has brought about renewed interest in thiolate bond formation as applied to nanostructures.

In this study, we investigated the kinetics of gold-thiolate bond formation on colloidal gold nanoparticles with the intention of elucidating the design parameters necessary to successfully prepare optical nanoprobes for biological sensing applications. The ligand-exchange process was characterized by monitoring the surface-enhanced Raman scattering (SERS) intensity of vibrational modes corresponding to specific thiolated Raman-active molecules. Whereas other techniques such as UV/vis absorption have been used to monitor time-dependent changes in the localized surface plasmon resonance during nanoparticle aggregation and gold-thiolate bond formation,[16] Raman spectroscopy's inherent chemical specificity allowed us to monitor both the changing surface chemistry and structural properties of the dynamically forming ligand shell. In order to prepare biologically relevant nanoprobes, we ensured that all Raman-active molecules were water soluble to maintain stability of the nanoparticles. Our results were compared with a theoretical model that predicted the effect of ensemble absorption and scattering of light during propagation through a turbid media.

SERS is a highly sensitive, chemically specific sensing modality that is well suited for studying the kinetics of gold-thiolate formation on nanoparticles. To date, however, only a few studies have specifically investigated the kinetics of ligand exchange on gold nanoparticles using SERS. One such study investigated ligand exchange using citrate-stabilized gold nanoparticles

dispersed in dimethylformamide (DMF).[17] This study primarily used reporter molecules with limited water solubility, making aggregation effects a larger concern. Additionally, the toxicity of DMF and the extra purification steps required to remove DMF makes these probes undesirable for rapid manufacturing. A different research group used time-dependent SERS and a ratiometric technique to quantify ligand exchange on simultaneously aggregating gold nanoparticles.[18] This technique, however, relies on the generation of hotspots, which can lead to unreproducible results due to uncertainty in the position of the molecular analyte with respect to the metal-metal junction. Additionally, it is impossible to fully decouple ligand exchange kinetics from aggregation kinetics using this approach. In this paper, we discuss ligand exchange kinetics and the design parameters necessary to prepare unaggregated, water-soluble gold nanoparticles for biological sensing applications.

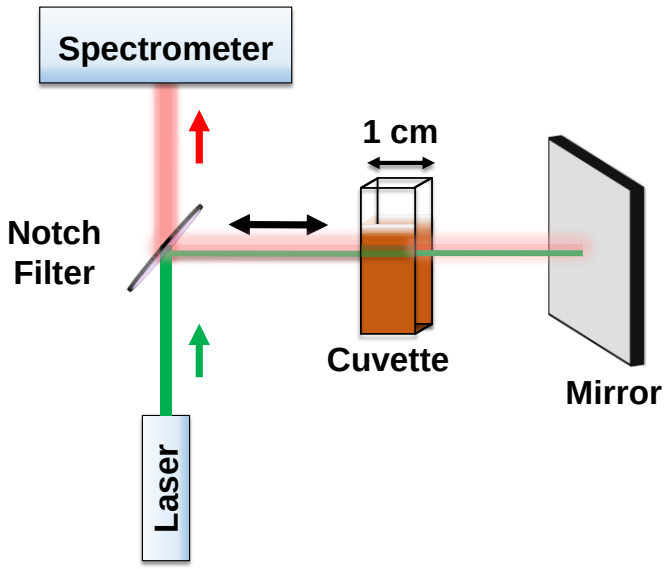

Figure 1. Schematic of backscattering collection geometry using a 1-cm-path-length cuvette. Raman scattered light was directed to a grating spectrometer after a holographic notch filter removed undesired Rayleigh scattered light.

Theory

The chemisorption of alkanethiol molecules to gold nanoparticles generally follows a first-order Langmuir adsorption model and is described by the following:[14]

$$\theta(t-t_0) = A(1-\mathrm{e}^{-k_{\mathrm{obs}}(t-t_0)}) \quad [2]$$

where θ is the fractional surface coverage, A is a constant dependent on the association or dissociation constants of the adsorption reaction, k_{obs} is the rate constant, and t_0 is a time delay factor added to account for the time required to mix the solution after the introduction of Raman reporter molecules. We assumed the binding characteristics of gold-thiolate bonds are similar in both aromatic thiolated reporter molecules and alkanethiol molecules such that the Langmuir adsorption model will appropriately describe chemisorption during ligand exchange. Furthermore, only colloidal nanoparticle measurements performed in a backscattering collection geometry were considered, as illustrated by Figure 1.

The kinetics of gold-thiolate bond formation were monitored using SERS. SERS, as has been discussed extensively,[19] operates on two distinct enhancement mechanisms: chemical enhancement and electromagnetic enhancement. Chemical enhancement is a weak effect and likely arises from a combination of resonances between the metal-molecule complex, deformation in the molecular polarizability, and electron charge transfer between molecules and the plasmonic surface.[20,21] In contrast, the stronger electromagnetic enhancement effect originates from the collective oscillation of the electron gas under resonant excitation. As a

limiting case, we only consider electromagnetic enhancement because it is a more useful design parameter and is several orders of magnitude stronger than chemical enhancement.

A selection rule for Raman spectroscopy is that the molecular polarizability must temporally deform or distort under excitation. The intensity of Raman scattered light may be described by three multiplicative terms. First, for molecular ensembles, the Raman scattering intensity is related to the number of molecules *N* present in the sampling volume and a factor $|\chi|^2$ where χ is the susceptibility of individual molecules. Because the susceptibility described here is related to the first-order Taylor expansion of molecular polarizability, the selection rule is satisfied. To accurately describe the Raman scattering intensity of molecules bound near the surface of a single plasmonic nanoparticle, a second term called the electromagnetic enhancement $G(\omega,\omega_0)$ is necessary. Here, ω corresponds to the Stokes shifted frequency of scattered light and ω_0 corresponds to the excitation frequency. The third and final term is crucial for plasmonic nanoparticle ensembles and is proportional to the Beer-Lambert law, which describes the exponential decay of light due to absorption and scattering (extinction) in turbid media. Therefore, the scattering intensity $I(\omega,\omega_0)$ as it propagates through a sample of thickness *b* may be defined as the following:[22,23]

$$I(\omega,\omega_0) = N|\chi|^2 G(\omega,\omega_0)\int_0^b dz\, e^{-zc[\varepsilon(\omega)+\varepsilon(\omega_0)]} \quad [3]$$

where *c* is the nanoparticle concentration and ε is the corresponding molar extinction coefficient.

To calculate the intensity of Raman scattering and kinetics of chemisorption, we first assumed spherical gold nanoparticles under the quasi-static approximation. Therefore, the electromagnetic enhancement is given by:[24]

$$G(\omega,\omega_0)=\left|\left[1+2g(\omega)\right]\left[1+2g(\omega_0)\right]\right|^2 \quad [4]$$

where g is the Clausius-Mossotti relation, $g=(m^2-1)/(m^2+2)$, and m is the ratio of the refractive index of gold to the refractive index of the surrounding media (water, n_0 = 1.33). Frequency-dependent optical constants for gold were obtained from Johnson and Christy.[25] The extinction cross section was calculated from the following:[26]

$$C_{\text{ext}}=4k\pi a^3\,\text{Im}\left\{\frac{m^2-1}{m^2+2}\right\}+\frac{8}{3}(ka)^4\,\pi a^2\left|\frac{m^2-1}{m^2+2}\right|^2 \quad [5]$$

where a is the radius of the nanoparticle and k is the wavevector ($k=2\pi n_0/\lambda_{\text{ex}}$) of the excitation light in the surrounding media.

We have previously demonstrated the importance of the Beer-Lambert law in calculating the Raman scattering intensity of nanoparticle ensembles.[22] Although the spontaneous Raman scattering intensity is intrinsically linear with respect to nanoparticle concentration, we have shown a nonlinear response due to optical extinction at higher nanoparticle concentrations. Incorporating the Beer-Lambert law with electromagnetic enhancement results in the following expression:[22]

$$R(\omega,\omega_0,\text{c})=R_0G(\omega,\omega_0)\frac{1-e^{-bn_0c[\varepsilon(\omega)+\varepsilon(\omega_0)]}}{n_0\varepsilon(\omega)+n_0\varepsilon(\omega_0)} \quad [6]$$

where R_0 is a constant dependent on the laser beam profile and the molecular Raman scattering cross section (*i.e.*, $N|\chi|^2$). From Eq. [6], it is apparent that nanoparticle concentration is responsible for the extinction of $R(\omega,\omega_0,c)$ and thus the nonlinear dependence is clear. It is possible, as a result, to optimize the concentration of nanoparticles in solution to obtain a maximal signal based on the extinction coefficient and path length.

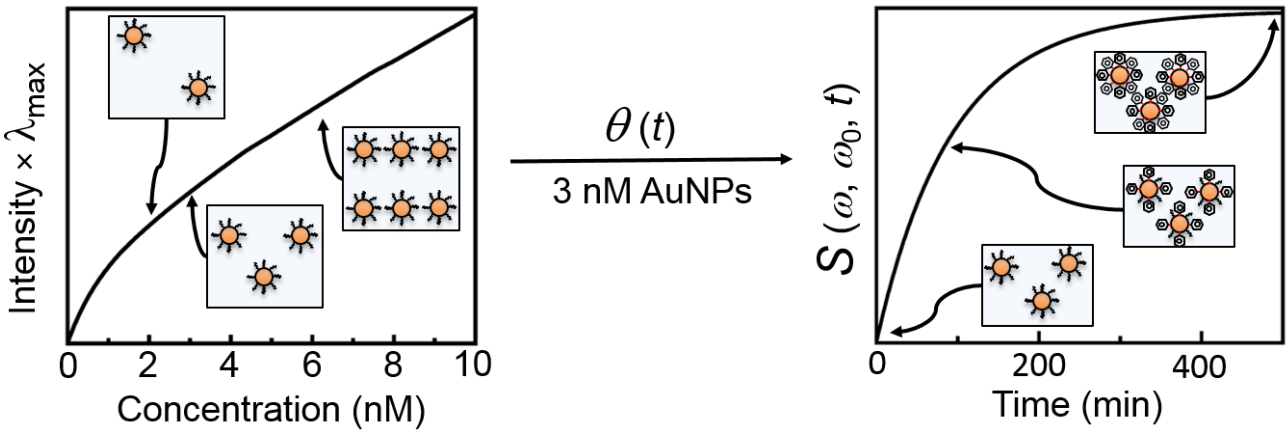

Figure 2. As illustrated by the Beer-Lambert law, the intensity of propagated light through turbid media decays exponentially. This intensity is a function of nanoparticle concentration as described by $R(\omega, \omega_0, c)$. Variation of (Intensity $\times \lambda_{max}$) with nanoparticle concentration is depicted on the left. A threshold concentration (3 nM and path length b = 1 cm) of nanoparticles was chosen as an idealized model. The number of adsorbed molecules $p(t)$ varied according to the first-order adsorption model $\theta(t)$ (k_{obs} = 0.01 min^{-1}, t_0 = 0 min) and was applied to the function $S(\omega,\omega_0,t)$, as shown on the right.

Ligand exchange kinetics may be described by modifying the previous equation to account for the adsorption of Raman-active reporter molecules as a function of time.[23] For non-resonant reporter molecules such as 2-thio-5-nitrobenzoic acid (TNB), the molar extinction (13,600 M^{-1}cm^{-1} at 412 nm)[27] is negligible in comparison with the molar extinction of gold nanoparticles (10^9 M^{-1}cm^{-1} at ~525 nm), such that we may neglect the extinction caused by these molecules even when they are added in molar excess. Thus, the kinetic equation to model

the adsorption of molecules to colloidal nanoparticles with a fixed nanoparticle concentration is given by:[23]

$$S(\omega,\omega_0,t) = S_0 G(\omega,\omega_0)\frac{p(t)}{c}\frac{1-e^{-bn_0c[\varepsilon(\omega)+\varepsilon(\omega_0)]}}{n_0\varepsilon(\omega)+n_0\varepsilon(\omega_0)} \quad [7]$$

where S_0 is a constant dependent on the laser beam profile and molecular Raman scattering cross section and $p(t)$ is the concentration of bound molecules. The time dependence of $S(\omega,\omega_0,t)$ was calculated by applying a first-order Langmuir adsorption model with parameters k_{obs} = 0.01 min^{-1} and t_0 = 0 min. In Figure 2, the intensity grows as a function of time for a fixed nanoparticle concentration of 3 nM. The effect described by $R(\omega,\omega_0,\mathrm{c})$ is a nonlinear response with nanoparticle concentration as predicted by Beer's law. When the turbidity of a solution (nanoparticle concentration) increases, light propagating through that solution decays exponentially (Eq. [6]). In contrast, for a constant nanoparticle concentration, the time-varying adsorption of weakly scattering molecules will have a linear response as described by $S(\omega,\omega_0,t)$ in Eq. [7]. This model provides confidence that it is possible to monitor the linear response of gold-thiolate bond formation in colloidal suspension.

Results and Discussion

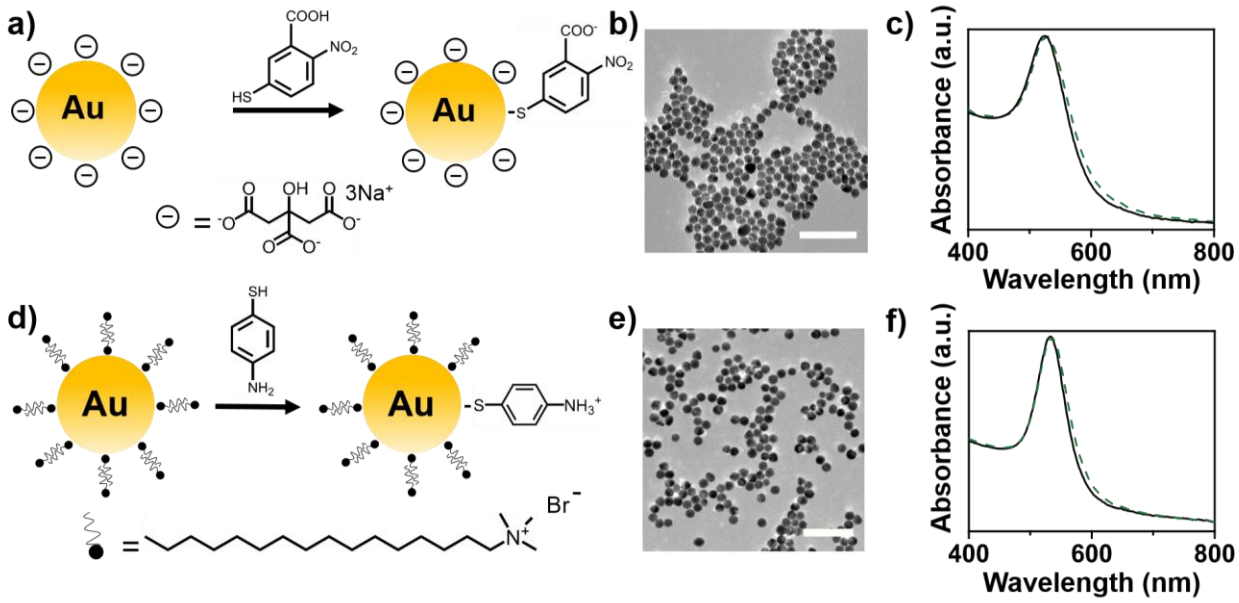

Figure 3. Schematic of the ligand exchange process. (a) Ligand exchange of citrate with TNB and (b) ligand exchange of CTAB with 4-ATP. Transmission electron micrograph of (c) citrate-stabilized (scale bar: 100 nm) and (d) CTAB-stabilized (scale bar: 200 nm) nanoparticles. UV/vis spectra of (e) citrate-stabilized and (f) CTAB-stabilized nanoparticles before (solid line) and 2 weeks after ligand exchange (dashed line).

We first synthesized 18-nm gold nanoparticles using the boiling citrate method. Monodispersity, shape, and size were verified through a combination of transmission electron microscopy (TEM), UV/vis spectroscopy, and dynamic light scattering (DLS) measurements. Citrate-stabilized gold nanoparticles are particularly attractive because of the relative ease in which the citrate ligands may be exchanged. Ellman's reagent or 5,5′-dithiobis-(2-nitrobenzoic acid) (DTNB) is a common Raman-active reporter molecule. DTNB's disulfide bond readily cleaves and forms 2-thio-5-nitrobenzoic acid (TNB) when dissolved in water at pH ~ 7. This may be monitored by measuring its absorbance at 412 nm.[28] As shown in Figure 3, ligand exchange was initiated by the introduction of aqueous TNB into a solution of gold nanoparticles. After ligand exchange was complete, each sample was stored at room temperature to ensure stability. Using UV/vis spectroscopy, we found no evidence of aggregation or coalescence (Figure 3c). Nanoparticle stability was further assessed by measuring ζ -potential and DLS.

Before ligand exchange, the citrate-stabilized nanoparticles had a ζ-potential of -29.0 ± 6.5 mV. After ligand exchange, the nanoparticles had a ζ-potential of -13.0 ± 2.1 mV, indicating electrostatic stabilization in suspension. DLS data are shown in the Electronic Supporting Information (Figure S1).

In addition, ligand exchange of 4-aminothiophenol (4-ATP) molecules was performed on 40-nm gold nanospheres stabilized with CTAB (Figure 3b). Whereas CTAB is notoriously difficult to remove from gold nanorods, CTAB is readily removed from the highly faceted gold nanosphere surface. We verified that the nanoparticles were stable before and after ligand exchange using UV/vis spectroscopy (Figure 3f) and ζ-potential/DLS. The ζ-potential before ligand exchange was 40.4 ± 1.1 mV and the ζ-potential after ligand exchange was 41.1 ± 2.9 mV. Likewise, the DLS data show no significant change in the size distribution of nanoparticles before and after exchange (Figure S1).

The kinetics of gold-thiolate bond formation were measured after introducing Raman-active reporter molecules TNB and 4-ATP into citrate-stabilized and CTAB-stabilized gold nanoparticle suspensions, respectively. Before introduction of reporter molecules, we adjusted the nanoparticle concentration such that the ratio of the number of available binding sites to the number of molecules was equivalent for both TNB/citrate and 4-ATP/CTAB solutions. Coverage density calculations were based on the assumption that TNB has a molecular footprint of 0.26 nm^2/molecule and 4-ATP has a molecular footprint of 0.20 nm^2/molecule.[29,30] Molecules were added in molar excess such that approximately 10^5–10^6 molecules per binding site were available before chemisorption took place.

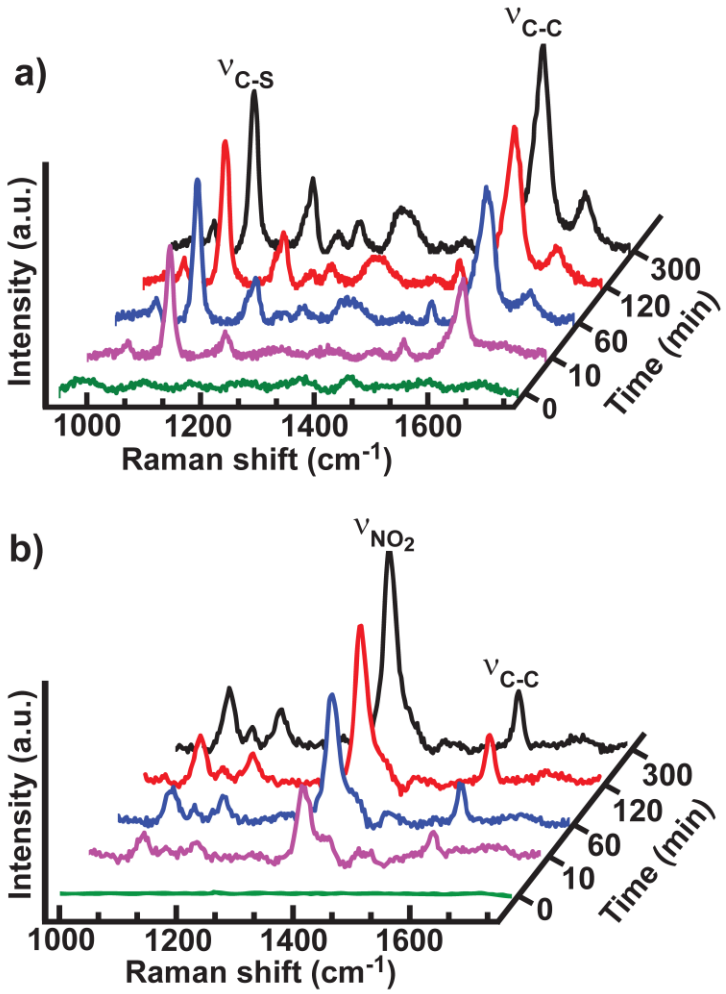

Figure 4. Kinetic SERS spectra of representative samples illustrating the growth of vibrational modes during ligand exchange of (a) CTAB with 4-ATP and (b) citrate with TNB. Reporter molecules were added immediately after t = 0 min.

The inherent chemical specificity of Raman spectroscopy allows simultaneous monitoring of the growth of multiple vibrational modes during ligand exchange. In Figure 4a, the kinetic SERS spectra of 4-ATP chemisorbed to gold nanoparticles is shown. Although CTAB-stabilized gold nanoparticles have an Au-Br band at 174 cm^{-1},[31] it was not possible to quantify the desorption of CTAB from spherical gold nanoparticles because the band immediately disappeared after introduction of 4-ATP. In contrast, we were able to monitor partial desorption of CTAB from gold nanorods when using a 785 nm excitation laser; however, this effect is likely due to the higher density and affinity for CTAB on the nanorod surface rather than a wavelength

dependent effect (Figure S2). The exceedingly weak signature of the Au-S bands at 240 and 480 cm^{-1} in colloidal measurements[32] made it challenging to directly measure the formation of gold-thiolate bonds using SERS. Instead, we monitored the time-dependent growth of stronger vibrational modes, which is correlated to the formation of gold-thiolate bonds as the molecules interact with the gold nanoparticle surface and displace electrostatically bound stabilizing ligands.

Previously, we demonstrated that SERS intensity varies nonlinearly with concentrations in colloidal suspensions of nanoparticles due to the competing mechanisms of optical extinction and electromagnetic enhancement (Eq. [6]).[22] As discussed in the theory section, Eq. [7] shows that the time-varying molecular adsorption component, $p(t)$, linearly varies with intensity. To verify this prediction, we performed ligand-exchange experiments and measured the growth of vibrational modes as a function of time. The relative growth of bands were measured (Figure S4) by computing an intensity ratio (area of band immediately after reporter molecule injection to area of band at the end of the measurement). We found the behavior of each band to be consistent across samples. For example, the non-fundamental mixed vibrational mode $\nu(C-C)+\beta(C-H)$ at 1,357 cm^{-1} (Figure S4) grew nearly twice that of the $\nu(C-S)$ and $\nu(C-C)$ vibrational modes. Certain modes, especially $\nu(C-S)$, were mostly insensitive to the number of molecules adsorbed to the nanoparticles (intensity ratio of 1.53 ± 0.22), likely because this mode has an intrinsically large Raman scattering cross section and how the molecules orient themselves with respect to the surface.

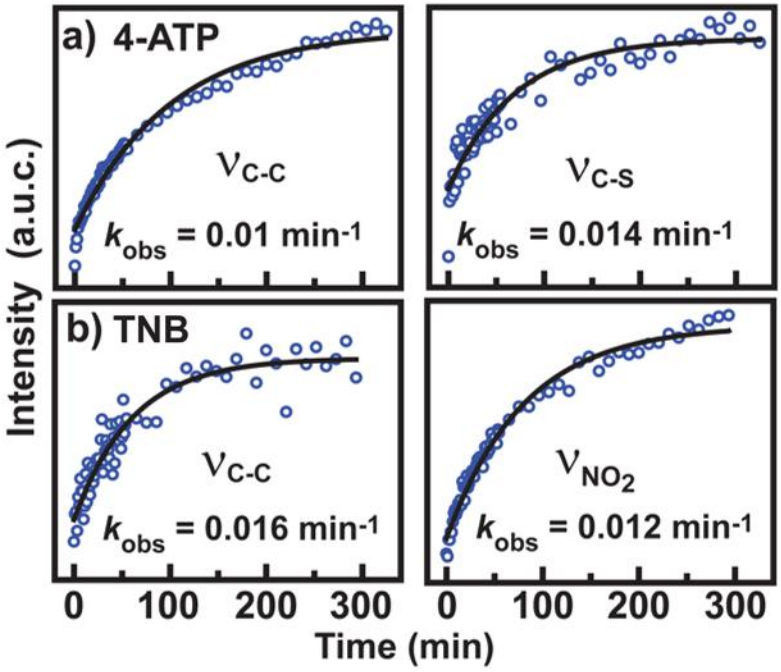

Figure 5. The SERS intensity as a function of time (circles) of strongly observed Raman bands of interest[29,30] were fit to a first-order Langmuir adsorption model (solid line). The rate constant k_{obs} for both (a) 4-ATP and (b) TNB molecules were found to have similar values, indicating that the stabilizing ligands have comparable affinities to gold.

Our results indicate that the chemisorption of TNB and 4-ATP may accurately be described by the first-order Langmuir adsorption model (Figure 5). Fitting of the experimental data to Eq. [2] for the stretching modes ν (C-C) (for 4-ATP) and ν (NO_2) (for TNB) are shown in Tables S1 and S2. We found that the average rate constant k_{obs} for both citrate and CTAB-stabilized gold nanoparticles was ~0.01 min^{-1} and, based on these data, we expect 90% surface coverage to be obtained approximately 4 hours after introduction of the Raman-active reporter molecules. Our results agree well with thiol adsorption kinetics on 3.3-nm gold nanoparticles as monitored by *in situ* time-resolved x-ray absorption fine structure (XAFS) where researchers measured a rate constant of 0.0132 min^{-1}.[33] They attributed a faster adsorption event during the first 20 minutes of measurement to adsorption on edges and corners. We did not observe this

event, possibly due to size differences between our nanoparticles and a lack differences in available defect sites. Other techniques such as x-ray photoelectron spectroscopy (XPS) have been used to quantify the ligand exchange and density of thiolated molecules on gold nanoparticles surfaces.[34] For the purpose of monitoring the dynamics of nanoparticle surface chemistry in solution, XPS is not an ideal technique because it requires that the sample consist of dried nanoparticle films.

The surface-area-to-volume ratio plays a huge role in the efficiency and speed of gold-thiolate formation. One of the most intriguing aspects of nanoscience is the modified characteristics of nanomaterials with respect to bulk materials. Researchers often observe that SAMs can take anywhere from 12–24 hours to form on clean, flat gold substrates.[35] For simplicity, if we assume a 1 μm^2 rectangular laser spot size illuminating a flat gold substrate, that same laser can probe 2,000 nanoparticles in a 1-cm path length at a concentration of 3 nM. Given that the surface-area-to-volume ratio of the nanoparticles probed in our experiments is on the order of 10^8, we see that colloidal measurements offer huge advantages over interrogating ~~many~~ flat surfaces. ~~simultaneously.~~ With this experimental setup, it also possible to probe fast kinetics. By reducing the integration time, we can probe fewer nanoparticles on a shorter time scale and investigate effects that occur rapidly. For example, we achieved an acceptable signal-to-noise ratio (~4.8) with an integration time of 50 ms for a monolayer of TNB-coated nanoparticles. With a 250-ms integration time, we recorded a signal-to-noise ratio of ~15.7. For the experiments discussed in Figures 4 and 5, we chose to investigate ensemble-averaged effects by probing large numbers of nanoparticles. To illustrate the differences in colloidal *versus* macroscopic substrate measurements, we took a flat gold substrate, added DTNB, and showed that even after 10 hours of measurements, SAM formation was not complete (Figure S2) and

minimal structural and orientation information could be obtained. In contrast, the ensemble-averaged kinetic nanoparticle spectra offer a rich array of structural information.

Additionally, the rate constant k_{obs} being insensitive to changes in reporter molecule concentration in both cases indicates that chemisorption of the molecules in molar excess are not controlled by a diffusion-limited process. The invariance in the rate constant across multiple vibrational modes and the consistent demonstration of the Langmuir adsorption profile for each mode indicates that wavelength-dependent optical extinction during chemisorption is negligible. This result matches our theoretical prediction where the Stokes shifted frequency ω is independent of the adsorbed chemical species $p(t)$. The fact that k_{obs} is similar for both processes implies that the stabilizing ligands (citrate, CTAB) have roughly equivalent affinity for gold nanoparticles. Although it has been reported that CTAB ligands have a stronger affinity for gold than citrate ligands, we found that this is only true for gold nanorods, not nanospheres.[11] Gold nanorods present specific facets (*i.e.*, {110}) that more strongly bind to CTA^+ micelles,[31] whereas gold nanospheres are highly faceted in nature and do not have large areas of exclusively {110} surface sites. Conversely, we found that additional purification and preparation steps were necessary to perform ligand exchange on gold nanorods (Figure S3).

Bands of interest were fit to Lorentzian distributions for further analysis. As shown in Figure 6, we observed spectral shifting of the center band frequency during chemisorption. Our theoretical model suggests that the intensity $S(\omega, \omega_0, t)$ of each Raman band is shift invariant during this process. In other words, as molecules adsorb to the nanoparticle surface, the band is not expected to shift as a consequence of any optical effects. This result, therefore, suggests that center band frequency shifting is a result of deformation of the molecular polarizability of

adsorbed molecules *via* a metal-molecule complex. Certain bands such as ν(C−S) exhibit minimal band shifting. As shown in Figure 6a, the ν (C-C) mode shifted from 1,601 cm^{-1} at t = 1 min to a steady-state Raman shift of 1,594 cm^{-1}. Similarly, the mode ν (C-C) + β (C-H) began at 1,376 cm^{-1} and reached a steady state of 1,357 cm^{-1}.

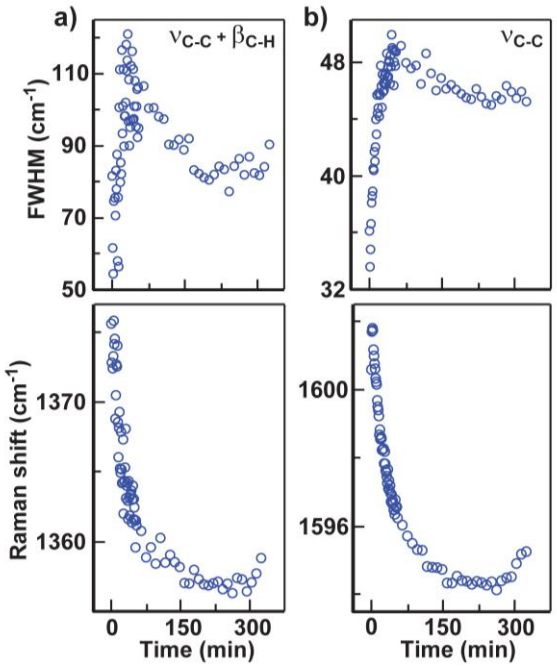

Figure 6. Time-dependent change in FWHM (top) and center band frequency (bottom) as determined by fitting to Lorentzian distributions. (a) Mixed mode ν(C−C)+β(C−H) and (b) fundamental mode ν(C−C). These data correspond to a representative sample (final 4-ATP concentration: 125 μM).

During gold-thiolate bond formation, the full width at half maximum (FWHM) grows and saturates within the first hour of introducing reporter molecules (Figure 6). Subsequently, the FWHM narrows to an intermediate steady-state position. This indicates that the initial molecules are disordered and slowly become more ordered until the majority of stabilizing CTAB ligands have been replaced. This effect is analogous to the formation of a SAM substrate.[35] The ligand exchange of citrate with TNB followed similar trends and is discussed in the Supporting

Information (Figures S6–S7). Blue-shifting of the center band frequency indicates a weakening bond. This is due to ligand-ligand, metal-molecule interactions, and orientation effects during monolayer formation. We are able to gain much insight from the data shown in Figures 5 and 6 regarding the state of the surface chemistry in the nanoparticle ensemble. The initial growth of Raman bands corresponds to molecular adsorption and eventually leads to chemisorption and reorientation of the molecular species on the nanoparticle surface. Because our data in Figure 5 corresponds well to the first-order Langmuir adsorption model, we can conclude that the majority of signal arises from the interaction and adsorption of new molecular species rather than molecular reorientation. While molecular reorientation is an important effect, its contribution to the signal intensity is likely minimal, as indicated by our theoretical model where we only assume adsorption increases the signal. That being said, molecular reorientation causes, in part, the shifting we observe in the center band frequency of certain Raman modes. To fully explore the effects of molecular reorientation, new methods such as observing the kinetics of partially ligand exchanged nanoparticles and polarization measurements, beyond the scope of this report are necessary. To further analyze the meaning of blue-shifting during chemisorption, we compared unbound 4-ATP molecules with bound 4-ATP molecules chemisorbed to a SAM of gold nanoparticles.

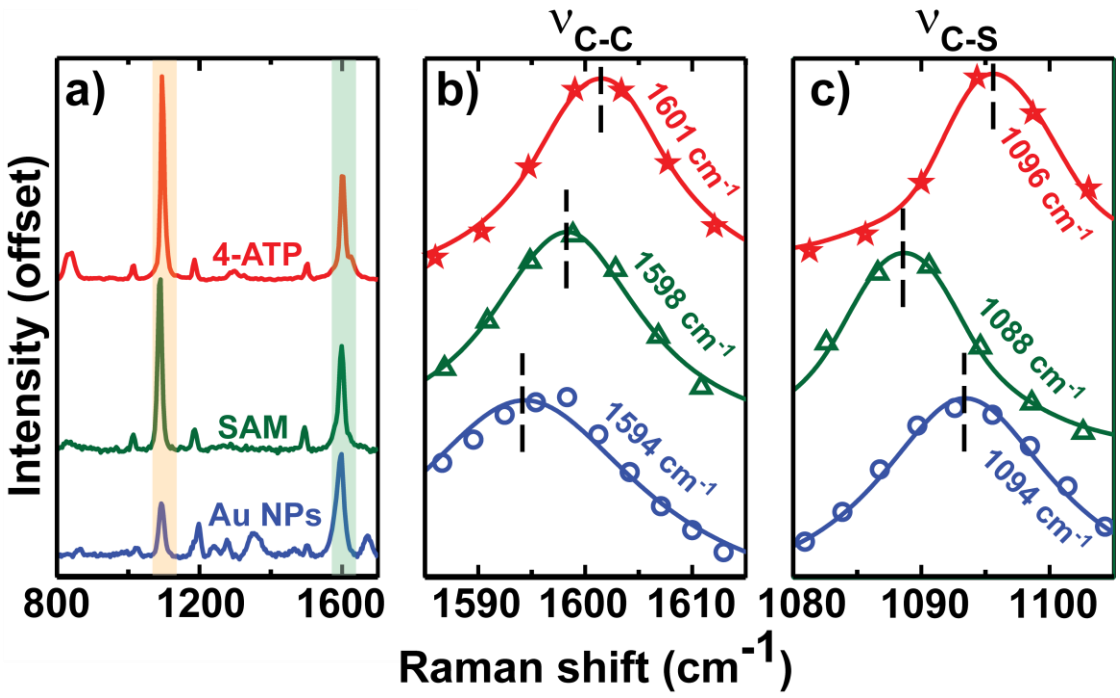

Figure 7. (a) Raman spectra of colloidal gold nanoparticles (blue, Au NPs) with chemisorbed 4-ATP, a self-assembled monolayer of gold nanoparticles on glass substrate with chemisorbed 4-ATP (green, SAM), and unbound 4-ATP molecules (red, 4-ATP). The spectra were normalized to the $\nu(C-C)$ mode. Lorentzian fit (solid line) and spectral data points for Au-NPs (circles), SAM (triangles), and 4-ATP (stars) for (b) $\nu(C-C)$ and (c) $\nu(C-S)$.

A self-assembled monolayer of gold nanoparticles on a glass substrate was fabricated to compare the center band frequency of 4-ATP molecules chemisorbed to gold in colloidal suspension *versus* dried substrate. This comparison allows to us monitor the binding strength of the respective thiolated molecules in solution as compared to dried substrates. Treatment of the vibrations of molecules as harmonic oscillators shows that longer Raman shifts correspond to more tightly bound molecules. On dried substrate, $\nu(C-C)+\beta(C-H)$ was not active; however, it was possible to compare $\nu(C-S)$ and $\nu(C-C)$, as shown in Figure 7. As previously mentioned, the $\nu(C-S)$ mode is largely shift invariant and insensitive to the number of bound molecules. Therefore, it is an excellent mode to obtain information about the state of binding. On

gold nanoparticles, $\nu(C-S)$ was blue-shifted from that of unbound 4-ATP molecules but red-shifted from the SAM configuration. This indicates that the C-S bond strength in colloidal gold nanoparticles is in between the SAM and free 4-ATP molecules; the 4-ATP molecules were most tightly bound to the dried substrate. The $\nu(C-C)$ mode was blue-shifted from both the unbound and SAM-bound 4-ATP molecules, indicating that there was significant deformation due to bonding in the C-C bonds of the aromatic ring. The blue shift past both the SAM and unbound 4-ATP in this mode may have arisen from the fact that this mode is more sensitive to the number of adsorbed molecules than the $\nu(C-S)$ mode. Nonetheless, based on these data we can conclude that gold-thiolate bond formation is occurring without the need for directly measuring Raman modes associated with Au-S vibrations. Additional experiments for measuring the kinetics of colloidal gold to the glass substrate were not performed because our primary interest was in measuring the binding kinetics and ligand exchange of thiolated molecules to the gold nanoparticle surface in solution. While it is technically possible to measure kinetic macroscopic substrate measurements with our experimental setup, we determined that the best way to prove gold-thiolate formation was to compare the center frequency of certain Raman bands in the colloidal kinetic data to dried substrate measurements.

Experimental

Materials. Cetyltrimethylammonium bromide (CTAB, >99%), sodium borohydride ($NaBH_4$, >99.99%), trisodium citrate ($Na_3C_6H_5O_7$, >99%), silver nitrate ($AgNO_3$, >99%), tetrachloroauric(III) acid ($HAuCl_4$, >99.999%), 5,5′-dithiobis-(2-nitrobenzoic acid) (DTNB, >95%), polystyrene sulfonate (PSS, 70 kDa), 4-aminothiophenol (4-ATP, >97%) and

hydroquinone (1,4-benzenediol, >99%) were purchased from Sigma-Aldrich and used without further purification. Glassware was cleaned with freshly prepared aqua regia (3:1 HCl:HNO_3) and rinsed with 18.2 MΩ-cm water multiple times.

Instrumentation. Raman spectra were acquired using a Horiba LabRAM HR 3D confocal microscope configured with 633 nm (8.5 mW at the sample) and 785 nm (110 mW at the sample) laser lines. A back-illuminated EMCCD (Andor, DU970P) was used for 633-nm experiments and a back-illuminated, deep-depletion CCD (Horiba Synapse) was used for 785-nm experiments. Unless noted otherwise, 633-nm laser excitation was used for Raman measurements. Spectra were acquired with a spectral resolution of 10 cm^{-1}. UV/vis absorption spectra were acquired with a Cary 5G spectrophotometer. Dynamic light scattering and ζ-potential measurements were acquired with a Malvern Zetasizer Nano ZS. Transmission electron microscopy was performed using a JEOL 2100 Cryo transmission electron microscope with an accelerating voltage of 200 kV.

Nanoparticle Synthesis. Citrate-stabilized gold nanospheres were synthesized using the boiling citrate method where 97.5 mL of H_2O was mixed with 2.5 mL of 0.01 M $HAuCl_4$. Under magnetic stirring, the solution was heated until boiling at which point 3 mL of 5% w/v citrate solution was added. The solution was allowed to boil for 5 minutes and slowly turned deep red. After cooling down, the solution was centrifuged at 5,250 × g for 3 hours to remove excess citrate. CTAB-stabilized gold nanospheres were synthesized using a seed-mediated method as described elsewhere.[36] Gold nanorods were synthesized using a recently developed seed-mediated method with hydroquinone as the reducing agent.[37] To remove bound CTAB from gold nanorods we used a chloroform extraction technique described by Wei and coworkers.[38] Briefly, we took 5 mL of OD 20 gold nanorods in H_2O and added 5 mL of chloroform. The immiscible

solvents were rapidly mixed for a minimum of 1 minute to form an emulsion and then centrifuged at 1,000 × *g* for 3 minutes. We then added 0.5 mL of 1% w/v PSS in H_2O and redispersed the pellet. After waiting 2 hours, centrifugation was repeated twice more to remove as much PSS-CTAB as possible. The sample was then centrifuged at 5,000 × *g* for 4 minutes in a 30,000 g/mol-molecular-weight-cutoff centrifuge filter. To the pellet, 1 mL of 1% w/v PSS was added. After 1 hour, the nanoparticles were centrifuged at 5,000 × *g* for 4 minutes and then redispersed in H_2O.

Substrate Fabrication. A clean glass slide was functionalized with 10 mM ethanoic (3-aminopropyl)-trimethoxysilane overnight. After rinsing multiple times with ethanol, a solution of citrate-stabilized gold nanoparticles (~4 nm diameter) was deposited on the substrate and allowed to dry for 2 hours. The substrate was rinsed with H_2O multiple times and allowed to air dry. A 10 mM 4-ATP solution (pH = 3) in H_2O was deposited onto the substrate and allowed to dry before Raman measurements were performed. For unbound 4-ATP measurements, an ethanoic solution of 50 mM 4-ATP was allowed to dry on a clean glass slide.

Kinetic Raman Measurements. Solution-phase samples (typically, 1.5–2 mL) were measured in a backscattering geometry with a 1-cm-path-length fused silica cuvette. Integration time varied between 10 to 20 seconds, depending on sample concentration. To initiate the kinetic measurements, Raman-active molecules were quickly added to a nanoparticle solution and rapidly mixed for approximately 30 seconds. Measurements began immediately after mixing.

Conclusion

Monitoring and understanding the kinetics of gold-thiolate bond formation is essential for the preparation of highly stable and robust gold nanoparticles. Covalent gold-thiolate bonds are superior over electrostatically bound molecules because electrostatic bonds are highly susceptible to diffusion and dissociation from the gold surface. Furthermore, maintaining the stability of gold nanoparticles in a variety of harsh ionic environments is critical for quantitative measurements.

Surface-enhanced Raman spectroscopy was used to indirectly monitor the kinetics of gold-thiolate bond formation. As a result of the intrinsic chemical specificity of Raman spectroscopy, it was possible to monitor the state of binding by analyzing the shift in center band frequency and FWHM by fitting a Lorentzian distribution to the collected data. Our results indicate that ligand exchange of citrate-stabilized and CTAB-stabilized gold nanospheres are well approximated by a first-order Langmuir adsorption model and have similar rate constants. Gold nanorods, in contrast, require additional purification steps and are challenging to fully exchange due to residual CTAB. We compared our results to an analytical model combining the Beer-Lambert law with electromagnetic SERS enhancement. The predictive model shows a linear relationship between chemisorbed molecules and Raman intensity, whereas a time-varying nanoparticle concentration is nonlinear in colloidal suspensions. Our experimental results were in excellent agreement with this model.

Acknowledgments

Brent M. DeVetter acknowledges support from the University of Illinois at Urbana-Champaign from NIH National Cancer Institute Alliance for Nanotechnology in Cancer

"Midwest Cancer Nanotechnology Training Center" grant R25 CA154015A. We also acknowledge support from a Beckman Institute seed grant and National Science Foundation grant CHE 0957849. Transmission electron microscopy, optical absorption spectroscopy, and DLS/ ζ -potential measurements were carried out in part at the Frederick Seitz Materials Research Laboratory Central Research Facilities, University of Illinois.

References

1 D. K. Gramotnev and S. I. Bozhevolnyi, *Nat. Photonics*, 2014, **8**, 13–22.
2 H. A. Atwater and A. Polman, *Nat. Mater.*, 2010, **9**, 205–213.
3 Y. Zhang, Y. Guo, Y. Xianyu, W. Chen, Y. Zhao and X. Jiang, *Adv. Mater.*, 2013, **25**, 3802–3819.
4 N. Tawil, A. Hatef, E. Sacher, M. Maisonneuve, T. Gervais, R. Mandeville and M. Meunier, *J. Phys. Chem. C*, 2013, **117**, 6712–6718.
5 J. V. Jokerst, T. Lobovkina, R. N. Zare and S. S. Gambhir, *Nanomed.*, 2011, **6**, 715–728.
6 D. A. Hines and P. V. Kamat, *ACS Appl. Mater. Interfaces*, 2014, **6**, 3041–3057.
7 H. Häkkinen, *Nat. Chem.*, 2012, **4**, 443–455.
8 M. Grzelczak, J. Pérez-Juste, P. Mulvaney and L. M. Liz-Marzán, *Chem. Soc. Rev.*, 2008, **37**, 1783–1791.
9 X. Qian, X.-H. Peng, D. O. Ansari, Q. Yin-Goen, G. Z. Chen, D. M. Shin, L. Yang, A. N. Young, M. D. Wang and S. Nie, *Nat Biotech*, 2008, **26**, 83–90.
10 Y.-C. Chang, C.-Y. Yang, R.-L. Sun, Y.-F. Cheng, W.-C. Kao and P.-C. Yang, *Sci. Rep.*, 2013, **3**.
11 X. Xia, M. Yang, Y. Wang, Y. Zheng, Q. Li, J. Chen and Y. Xia, *ACS Nano*, 2012, **6**, 512–522.
12 J. C. Love, L. A. Estroff, J. K. Kriebel, R. G. Nuzzo and G. M. Whitesides, *Chem. Rev.*, 2005, **105**, 1103–1169.
13 R. Berger, E. Delamarche, H. P. Lang, C. Gerber, J. K. Gimzewski, E. Meyer and H.-J. Güntherodt, *Science*, 1997, **276**, 2021–2024.
14 D. S. Karpovich and G. J. Blanchard, *Langmuir*, 1994, **10**, 3315–3322.
15 L. L. Rouhana, M. D. Moussallem and J. B. Schlenoff, *J. Am. Chem. Soc.*, 2011, **133**, 16080–16091.
16 M. G. Bellino, E. J. Calvo and G. Gordillo, *Phys. Chem. Chem. Phys.*, 2004, **6**, 424–428.
17 Y. Feng, S. Xing, J. Xu, H. Wang, J. W. Lim and H. Chen, *Dalton Trans.*, 2009, **39**, 349–351.
18 D. Zhang and S. M. Ansar, *Anal. Chem.*, 2010, **82**, 5910–5914.
19 B. Sharma, R. R. Frontiera, A.-I. Henry, E. Ringe and R. P. Van Duyne, *Mater. Today*, 2012, **15**, 16–25.
20 N. Valley, N. Greeneltch, R. P. Van Duyne and G. C. Schatz, *J. Phys. Chem. Lett.*, 2013, **4**, 2599–2604.
21 M. Moskovits, *Phys. Chem. Chem. Phys.*, 2013, **15**, 5301–5311.

22 T. van Dijk, S. T. Sivapalan, B. M. DeVetter, T. K. Yang, M. V. Schulmerich, C. J. Murphy, R. Bhargava and P. S. Carney, *J. Phys. Chem. Lett.*, 2013, **4**, 1193–1196.
23 D. F. Shriver and J. B. R. Dunn, *Appl. Spectrosc.*, 1974, **28**, 319–323.
24 M. Kerker, D.-S. Wang and H. Chew, *Appl. Opt.*, 1980, **19**, 4159–4174.
25 P. B. Johnson and R. W. Christy, *Phys. Rev. B*, 1972, **6**, 4370–4379.
26 C. F. Bohren and D. R. Huffman, *Absorption and Scattering of Light by Small Particles*, 2007.
27 G. T. Hermanson, *Bioconjugate Techniques, Second Edition*, Academic Press, 2nd edn., 2008.
28 H. Peng, W. Chen, Y. Cheng, L. Hakuna, R. Strongin and B. Wang, *Sensors*, 2012, **12**, 15907–15946.
29 B. Küstner, M. Gellner, M. Schütz, F. Schöppler, A. Marx, P. Ströbel, P. Adam, C. Schmuck and S. Schlücker, *Angew. Chem. Int. Ed.*, 2009, **48**, 1950–1953.
30 X. Hu, T. Wang, L. Wang and S. Dong, *J. Phys. Chem. C*, 2007, **111**, 6962–6969.
31 B. Nikoobakht and M. A. El-Sayed, *Chem. Mater.*, 2003, **15**, 1957–1962.
32 G. J. Kluth, C. Carraro and R. Maboudian, *Phys. Rev. B*, 1999, **59**, R10449–R10452.
33 H. Cheng†, L. Yang†, Y. Jiang, Y. Huang, Z. Sun, J. Zhang, T. Hu, Z. Pan, G. Pan, T. Yao, Q. Bian and S. Wei, *Nanoscale*, 2013, **5**, 11795–11800.
34 M. D. Torelli, R. A. Putans, Y. Tan, S. E. Lohse, C. J. Murphy and R. J. Hamers, *ACS Appl. Mater. Interfaces*, 2015, **7**, 1720–1725.
35 C. Vericat, M. E. Vela, G. Benitez, P. Carro and R. C. Salvarezza, *Chem. Soc. Rev.*, 2010, **39**, 1805–1834.
36 X. Wu, T. Ming, X. Wang, P. Wang, J. Wang and J. Chen, *ACS Nano*, 2009, **4**, 113–120.
37 L. Vigderman and E. R. Zubarev, *Chem. Mater.*, 2013, **25**, 1450–1457.
38 A. P. Leonov, J. Zheng, J. D. Clogston, S. T. Stern, A. K. Patri and A. Wei, *ACS Nano*, 2008, **2**, 2481–2488.